Meteoritics & Planetary Science 31, 502–517 (1996)

The fall of the St-Robert meteorite

PETER BROWN[1]*, ALAN R. HILDEBRAND[2], DANIEL W. E. GREEN[3], DENIS PAGÉ[4], CLIFF JACOBS[5], DOUG REVELLE[6], EDWARD TAGLIAFERRI[7], JOHN WACKER[8] AND BOB WETMILLER[9]

[1]Department of Physics, University of Western Ontario, London, Ontario N6A 3K7, Canada
[2]Geological Survey of Canada, Natural Resources Canada, Continental Geosciences Division, 1 Observatory Crescent, Ottawa, Ontario K1A 0Y3, Canada
[3]Smithsonian Astrophysical Observatory, 60 Garden Street, Cambridge, Massachusetts 02138, USA
[4]Royal Astronomical Society of Canada Québec Centre, 7642 Boul. Shaughnessy, Montreal, Québec H2A 1K4, Canada
[5]Sandia National Laboratories, Org. 5909, Mail Stop 0978, P.O. Box 5800, Albuquerque, New Mexico 87185, USA
[6]Los Alamos National Laboratories, P.O. Box 1663, Los Alamos, New Mexico 87545, USA
[7]ET Space Systems, 5990 Worth Way, Camarillo, California 93012, USA
[8]Battelle, Pacific NW Laboratories, Richland, Washington 99352, USA
[9]Geological Survey of Canada, Natural Resources Canada, Pacific Division, 1 Observatory Crescent, Ottawa, Ontario K1A 0Y3, Canada
*Correspondence author's e-mail address: peter@danlon.physics.uwo.ca

(Received 1995 November 15; accepted in revised form 1996 April 16)

Abstract–The St-Robert (Québec, Canada) meteorite shower occurred on 1994 June 15 at 0h02m UT accompanied by detonations audible for >200 km from the fireball endpoint. The fireball was recorded by visual observers in Vermont, New York State, New Hampshire, Québec and Ontario as well as by optical and infrared sensors in Earth-orbit. Penetration to an altitude of 36 km occurred ~60 km to the northeast of Montreal, where the bolide experienced several episodes of fragmentation. A total of 20 fragments of this H5 chondrite, comprising a total mass of 25.4 kg, were recovered in an ellipse measuring 8 × 3.5 km. One fragment of the shower partially penetrated the aluminum roof of a shed.

Interpretation of the visual and satellite data suggests that the fireball traveled from south-southwest to north-northeast, with a slope from the horizontal of 55°–61°. A statistical evaluation of the likely heliocentric orbits for the body prior to collision with the Earth, coupled with theoretical modeling of the entry, suggests an entry velocity in the range of 12.7–13.3 km/s; the meteoroid had moved in a low-inclination orbit, with orbital perihelion located extremely close to the Earth's orbit.

From satellite optical data, it is found that the photometric mass consumed during the largest detonation is ~1200 kg. Estimation of the amplitude of the acoustic signal detected by the most distant observer yields a source energy near 0.5 kt TNT equivalent energy, which corresponds to a mass of order 10 metric tonnes. This measure is uncertain to approximately one order of magnitude. Theoretical modeling of the entry of the object suggests a mass near 1600 kg. Cosmogenic radionuclide activities constrain the lower initial mass to be ~700 kg with an upper limit near 4000 kg. Seismic data possibly associated with the fireball suggest extremely poor coupling between the airwave and the ground.

The total mass estimated to have reached the ground is ~100 kg (in material comprising >55 g fragments), while the preatmospheric mass is found to be most probably in the range of 1200–2000 kg.

INTRODUCTION

Knowledge of the flux of large meteoroids into the Earth's atmosphere is our primary means of characterizing their population in the near-Earth environment, which, in turn, can provide constraints on the evolution of the solar system's population of asteroids and comets. Recent data releases from the defense satellite systems illustrate the value of their observations in assessing the population of meteoroids below the limit of telescopic detection (*e.g.*, Tagliaferri *et al.*, 1994; McCord *et al.*, 1995), which have been observed in the diameter range of 0.5 to 5 m. The fall of the St-Robert meteorite has provided an opportunity to combine satellite observations of a large meteoroid fireball with constraints derived from eyewitness accounts, a well mapped meteorite strewn field, and analyses of some of the recovered meteorites.

On the evening of 1994 June 14 at 20h02m EDT (0h02m UT, June 15) a bright fireball was observed widely over the region encompassing upper New York State, Vermont, New Hampshire, Ontario and the southern portion of the province of Québec. Most residents in southern Québec did not witness the fireball but rather heard the sound detonations accompanying its passage. Shortly after the fireball's appearance, a 2 kg meteorite was removed from a shallow plunge pit east of the village of St-Robert, 60 km northeast of Montreal. Subsequent field work and local collection during the summer of 1994 located at least an additional 19 fragments within a "fall ellipse" measuring 8 × 3.5 km.

This fall constitutes the 47th authenticated meteorite recovered in Canada, the 3rd in the province of Québec, and the 12th recorded fall in the country (White, 1984). The associated strewn field is well delineated with more recovered fragments than any other Canadian fall except Bruderheim (Folinsbee and Bayrock, 1961).

Only four meteorites have well-determined orbits: Pribram, Lost City, Innisfree and Peekskill (Ceplecha, 1961; McCrosky *et al.*, 1971; Halliday *et al.*, 1978; Brown *et al.*, 1994). While recovery of meteorites shortly after falls is relatively common, the instances where sufficient visual observations of the fireball have been collected to allow determination of an approximate atmospheric path and a potential orbit are small (Jenniskens *et al.*, 1992). As a result, our knowledge of the orbital characteristics of meteorite-producing asteroids in the solar system before collision with Earth is still poor.

Here we determine the preatmospheric orbit for the St-Robert meteoroid by analysing visual and satellite observations of the fireball. The meteoroid's preatmospheric mass is independently derived from fireball observations and the terminal detonation of the fireball. Quick recovery allowed early gamma-ray spectrometer counts to detect short-lived isotopes, and measurement of 14 fragments in this manner yields an independently derived minimum and maximum preatmospheric mass of the St-Robert meteoroid.

THE FIREBALL

Visual Observations

Of the thousands of fireball eyewitnesses, a total of 66 were interviewed by at least one of the authors, and measurements were taken of the beginning and ending point of the fireball using a compass and clinometer. Apparent slopes, with respect to the ground, of the path of the fireball in the sky were also measured (independently), and a variety of other secondary information was collected. The time of occurrence of the fireball (20h02m EDT) was near local sunset, with the Sun at ~5° elevation and azimuth 297°. As a result, many Québec witnesses saw only the extensive dust cloud present after the fireball was subluminous, this circumstance applied in particular to observers near the ellipse of fall where most looked skyward only after hearing the loud detonations.

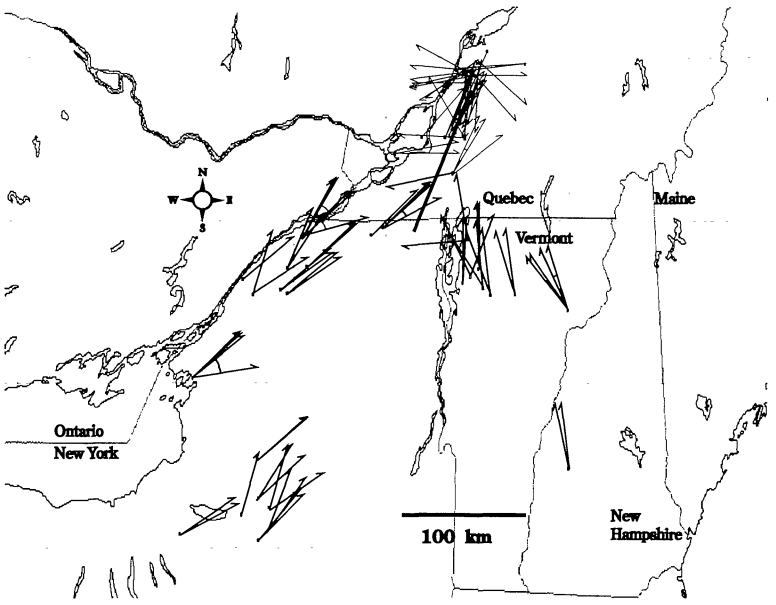

FIG. 1. Observer estimates for the azimuth for the beginning and ending of the fireball. Bold lines are observations of the fireball while lighter lines near the ellipse refer to the location of the main dust cloud only.

The tubular dust cloud was described as grayish-blue near the endpoint of the fireball, which some estimated lasted 30 min after the fireball's passage. Several observers noted that the cloud had two or three "bulges" or "puffs" near the endpoint, which may indicate that several episodes of gross fragmentation occurred before the terminal point. A handful of witnesses also mentioned specifically the similarity in appearance between this dust cloud and the explosion cloud left behind after the Shuttle Challenger accident, which suggests that many smaller "vapor trails" emanated from the main explosion. Most observers reported the fireball to be white in color, changing to yellow or orange near the endpoint, and most agreed that it was much brighter than the full Moon.

The azimuths for the fireball reported by all 66 observers are plotted in Fig. 1. The distribution of observers is far from ideal; most were some distance to one side of the fireball trajectory and, hence, provide only a very rough indication of the ground path. Many observers recorded the fireball only over the last 100 km of its path. This effect is due to the tendency of meteorite-producing fireballs to reach maximum light when relatively low in the atmosphere (Wetherill and Revelle, 1981) coupled in this case with essentially a daylight-brightness sky background and additional brightening due to fragmentation near the endpoint.

Several methods exist to determine the atmospheric trajectory of a fireball. For accurately measured trajectories obtained from multiple stations by photographic techniques, the beginning and ending points of the fireball path can be used from each station to define a plane that contains the fireball path. By computing the intersection lines of planes from two stations at a time, one can establish an average trajectory (Ceplecha, 1987). This is a useful method when very accurate data are available but is not very suitable for fireballs observed only visually.

A second, commonly employed method for visual observations uses the beginning and end points measured from all observers and calculates a path based on a least-squares determination of the intersection of these direction vectors (Borovicka, 1990). In this case, it becomes possible to reject obvious outliers without regard to observer, use as many points along the trajectory as each observer can identify (fragmentation points, *etc.*), and then maximize the agreement within the dataset in a least-squares fashion. Variations of this method, which use differing weights for each datapoint according to factors such as viewing geometry, have also been presented (*cf.*, McIntosh and Douglas, 1967).

In all these cases, attempts are made to process visual data, treating each case in an equivalent manner. The visual data collected for a given fireball has a vast range of quality, and frequently fortuitous circumstances make a small subset of the observations much more valuable than the remainder.

Since visual data are inherently inaccurate and debased by systematic errors, we have chosen to solve for the fireball trajectory in a straightforward graphical manner. In this procedure, intersecting azimuth lines are first used to establish a best-fit ground trajectory. Then the height is computed at which each altitude measurement intersects a vertical plane defining the ground-trajectory, taking into account Earth curvature. The slope of the fireball path is then determined by least-squares fitting the best height- *vs.* ground-distance measurements.

In the case of the St-Robert fireball, a fortunate alignment of careful observers directly under the ground path of the fireball, some 40 km from the endpoint, aided in the determination of a very precise estimate of the azimuth of the trajectory. These five observers, who were spread equidistant over a 15 km line perpendicular to the fireball path, show the expected variations in the slope of the trajectory from the horizontal and apparent direction of motion of the fireball if its ground-path is taken to lie almost directly in the middle of this observer line. The solution thus derived for the ground path is consistent with the majority of other observations and the general orientation of the fall ellipse, and this provides a formal solution for the azimuth of the apparent radiant of 202° ± 5°.

The solution for the slope of the apparent path in the atmosphere (with respect to the ground) using the graphical method is 20°, but the data allow a wide-range of values centered ~15°–35°. The duration of the event as measured by most observers ranged from 1–6 s, which suggests a steeper path. Halliday *et al.* (1989a) derived a relation between duration and entry angle from MORP data for those fireballs that were most likely to have produced meteorites. Using his relation and our best slope value of 20° results in an expected total duration of 9 s. To match our reported durations, one requires a slope >40°, which suggests that the large scatter in the slope values from the visual observations is indicative of a steeper trajectory.

From the visual dust-cloud and the fireball-trajectory observations, the best solution for the detonation height is 15 ± 5 km at a ground location of $\lambda = 73.07° \pm 0.05°$W longitude and $\varphi = 45.83° \pm 0.05°$N latitude. This visually determined detonation point is above the town of Michaudville.

Space-Based Sensor Detection

Infrared–The St-Robert meteoroid was detected near the end of its trajectory by space-based infrared and visible sensors operated by the U. S. Department of Defense. These sensors are described in limited detail elsewhere (Tagliaferri *et al.*, 1994). The sensors detect fireballs with some facility. However, the amount of information about the sensors that can be released is limited.

In this case, the infrared (IR) sensors detected the object during the last 1/2 s prior to its detonation, and both the IR and visible sensors observed the detonation of the object.

It is not possible to deduce the heading of the object with a high degree of certainty using just the IR. However, it is possible to derive a significant amount of information about the event if one assumes a heading of 202° for the trajectory as deduced from the ground-based observations.

It appears that as the object penetrated into the atmosphere, it started to break up at ~37.5 km altitude and detonated at 36.2 (±1.5) km. The detonation occurred over a point on the ground at ~45.8° N, 73.0° W. At the time the space-based sensors observed the event, the angle of descent was 58° from the horizontal.

Based on the time of detonation determined by the visible wavelength sensors, it is possible to estimate the velocity of the object to be ~12.2 km/s over this portion of its trajectory.

An interesting point from the IR observations is that after the detonation, the fireball appeared to continue downward for a short time and extinguished at ~33.6 km altitude.

Optical–The St-Robert fireball was also observed by high-altitude satellite optical sensors. These sensors respond to intense optical transients (*i.e.*, lightning, sunglint, and fireballs).

The observed peak total radiant power and radiant energy of the fireball were estimated as 5×10^{10} W and 1.3×10^{10} J, respectively. These estimates were made from the transient waveform (Fig. 2) recorded by the satellite sensors. This peak power corresponds to a visual magnitude of –18. The time of peak intensity occurred at 00:02:26 UT. The meteoroid's kinetic energy based on thermal energy radiated is 1.3×10^{11} J as discussed below. This corresponds to ~1500 kg of mass traveling with a velocity of 13 km/s.

The precise interpretation of the recorded waveform was made difficult because of poor signal to noise ratio. Initially it was thought that the leading shelf and the trailing step also represented signal from the fireball, but a closer examination of the sensor output both before and after the event revealed low-frequency noise of the same amplitude and character. These amplitude and energy estimates exclude these features of the waveform.

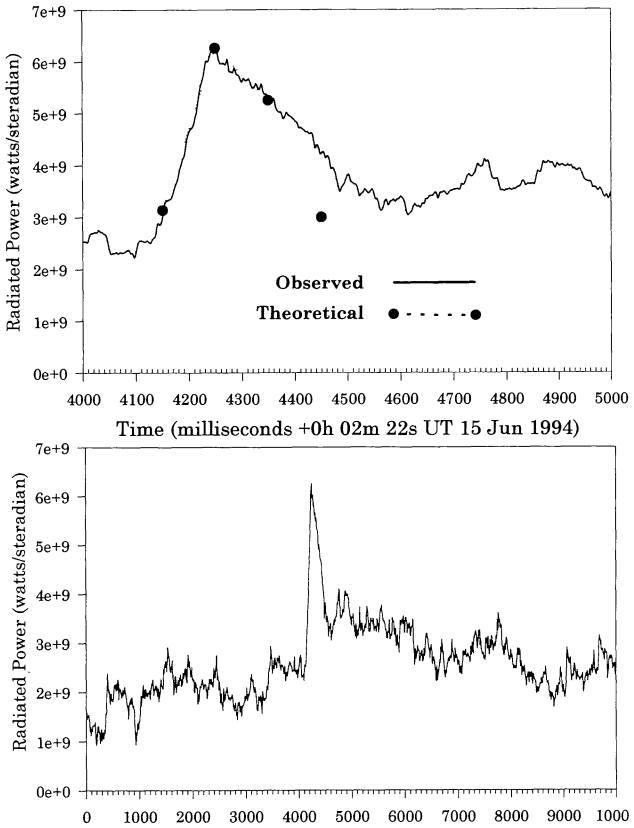

FIG. 2. Optical light curve of the detonation of St-Robert as seen from orbit. The large points (top graph) represent the equivalent luminosities in bins of 0.1 s derived from the theoretical light curve. The lower graph shows sensor output for the 10 s interval centered about the flash from the fireball.

These estimates assume first that the fireball temperature was ~6000 K and second, that 10% of the kinetic energy lost was radiated thermally. Estimates of the kinetic energy radiated thermally from bolides range from 1–30% based on comparisons with other phenomena. For instance, an atmospheric nuclear detonation radiates ~30% of its energy thermally. McCord *et al.* (1995), based on personal communication with G. Wetherill, suggest an average conversion efficiency of nearly 10% (McCord *et al.*, 1995).

The satellite optical sensors use Si detectors that respond to electromagnetic radiation between 400 and 1100 nm. These photovoltaic Si detectors response to a blackbody source is near maximum for a 6000 K source and is ~40% of its peak responsivity of 0.65 A/W at 900 nm. Its response is less for blackbody temperatures that are both greater than and less than 6000 K. Thus, assuming a 6000 K source results in a more conservative estimate of the fireball signal. Spectral modelling of several bright fireballs has shown that the meteor head typically has a temperature of 4000–5000 K (Borovicka, 1993, 1994).

The fireball radiant intensity, I, in watts per steradian was calculated as follows:

$$I = \frac{iD^2}{RF} \qquad \text{Eq. (1)}$$

where i is the Si signal current in amperes per square centimeter of sensor aperture, D is the satellite to fireball distance in centimeters,

R is the detector peak responsivity in amperes per watt and F is the fraction of the radiated power detected (0.40). The total energy radiated is then:

$$E = 4\pi \int I dt \qquad \text{Eq. (2)}$$

The total energy received outside the Earth's atmosphere from a star of bolometric magnitude 0.00 is equal to 2.48×10^{-12} W/cm^2. The bolometric magnitude and the apparent visual magnitude of a star with surface temperature similar to the Sun are the same (Allen, 1973). Thus, we may calculate the bolometric magnitude of the fireball and also identify its visual magnitude as we have assumed an apparent temperature similar to the Sun's.

The fireball intensity is converted to irradiance at a standard distance of 100 km before conversion to bolometric magnitude. Thus:

$$M_{bol} = -2.5\log\left[\frac{I}{10^{14} \times 2.48 \times 10^{-12}}\right] \qquad \text{Eq. (3)}$$

$$M_{bol} = 6 - 2.5\log I \qquad \text{Eq. (4)}$$

Source Energy Evaluation using Acoustic Information

Two reports from the city of St. Jean, 80 km from the endpoint, noted that a "whistling sound" was heard simultaneous to the flight of the fireball and lasted 3–4 s (of the ~6 s total duration of the event) near the end of the trajectory. One observer was drawn to look up after first hearing the sound. Such electrophonic reports have been discussed in detail by Keay (1992) and are commonly associated with large fireballs.

Residents of the area near the fall uniformly reported hearing a loud detonation, and in some cases 3–4 loud bangs preceding or following the main detonation. Multiple detonations were heard as far as 30 km from the fall ellipse; outside of this region all sound reports refer to one loud detonation only. Two possible explanations for these multiple sounds are sonic booms produced by individual fragments or enhancements in the ablational shock wave resulting from several episodes of fragmentation near the endpoint. Analysis of air waves from other large fireballs has yielded evidence that some are produced by point sources, while others are consistent with a cylindrical shock wave associated with the ballistic shock from the main body of the meteoroid (*cf.*, Cumming, 1989). The separate bangs were invariably depicted as fainter than the main detonation, which is suggestive of a rapid decline in audibility beyond the immediate fall area. Darkflight modeling indicates that subsonic speeds would be reached by even the largest of the known fragments within a few seconds of subluminous flight, only 2–3 km below the terminal point, which suggests that sonic booms would be localized to the region near the terminal point. Unfortunately, there is not enough data to distinguish between sonic booms from individual fragments or several fragmentations as the more likely explanation for these multiple sounds.

From the witness descriptions of the St-Robert event, we can deduce several basic properties concerning these audible sounds. Taking the most distant observer as a benchmark, we can establish the signal velocity to be ~295 m/s, which is found by taking the horizontal distance from the source to the most distant observer (230 km) and the earliest arrival time noted by the observer (13 min after the event). The total signal duration is taken to be 4 s in accordance with the observer's report and the signal amplitude is chosen to be 0.15 mbar; this is the minimum detectable overpressure for the human ear at low frequencies.

These signals are characteristic of ozonospheric acoustic returns. These are sounds generated by the bolide that were subsequently refracted downward by the higher temperatures (sound speeds) and stronger winds at 50 km altitude as compared to the values for both quantities lower in the atmosphere. On the basis of this type of return, we make the following assumptions in order to make a rough estimate of the bolide source energy. We present the acoustic analysis in detail so that it may easily be duplicated for future events by others—in the present case lack of instrumental recordings make the final results highly uncertain. For source altitudes above one scale height, significant corrections need to be applied to the results determined below. The net effect is that the estimated source energies below are lower limits to the true value if the real source height is $>>H_s$, as we believe to be the case for St-Robert, where H_s is the density scale height (~10 km in the troposphere). We have assumed also that atmospheric absorption is negligible. This is a reasonable assumption since the fundamental frequency of the blast wave decreases as the source energy increases, and, hence, absorption processes are much less important except for very great ranges or very high-altitude refractions.

First, we assume that the detonation was a low-altitude point source type explosion ($z << H_s$). Both line and point sources have applicability to meteor sound events (Revelle, 1976), but sound channeling to great range changes the character of the signal eventually to a cylindrical decay law. The uncertainty in the source energy estimation is limited by real natural atmospheric variability over short time scales (*i.e.*, tens of minutes; Reed, 1966). Consequently, using amplitude information alone can introduce large uncertainties in these results.

We also assume that a human observation of perceived signal loudness can be translated into a corresponding sound pressure amplitude. In this case, the sounds at ~230 km from the detonation point of the bolide were perceived as being a faint boom. Astapovich (1946) has used this concept to determine the acoustic efficiency factor (fraction of kinetic energy at explosive detonation which turns into sound), which is estimated to be 0.01%. Numerous discussions of the audibility of sonic-boom type sounds can be found in Zepler and Harel (1965); Hilton *et al.* (1972); Henderson and Hilton (1974a,b); and Gold and Soter (1979). The perceived sound levels corresponding to range and assumed altitudes here are consistent at the limits of human audibility with the distinction of a loudness of 120 dB (relative to 2×10^{-4} μbar) as being 0.15 mbar at a frequency limit of ~10 Hz.

We will evaluate the source energy of the bolide by three methods, namely an inversion of the empirical wind-corrected, amplitude-range-yield relation of Davidson and Whitaker (1992), an efficiency approach similar to that in Astapovich (1946) and in Cox (1958) and a line-source approach building on the work of Revelle (1976).

Empirical Approach

Several theoretical and empirical schemes have been proposed to evaluate amplitude of the acoustic signal for low-altitude sources (DuMond *et al.*, 1946; Reed, 1972; Revelle, 1976; Reed, 1977; Davidson and Whitaker, 1992). We have decided that the Davidson and Whitaker relation is the most reliable for ozonospheric returns when wind effects are significant. As previously discussed, this relation assumes that the signals are traveling in a cylindrical duct. Thus, the point-like nature of the source behavior is retained for ducted sound observations. For the time of year of the St-Robert event, ozonosphere winds are expected to be quite strong from the east, and consequently these winds will have significantly amplified the

perceived ground-level signals. Solving for their amplitude, source energy relation, for a source above the ground we find:

$$W = 1.35\times 10^{-7}\,\Delta P_{p-p}{}^{1.471}\,10^{-0.02588V}\,R^2 \qquad \text{Eq. (5)}$$

where W is the source energy in kilotonnes (kt) (for nuclear explosions), ΔP_{p-p} is the peak to peak value for the sound pressure in microbars, V is the magnitude of the ozonospheric wind in meters per second and R is the horizontal range to the event in kilometers.

For the St-Robert event, we have an estimated peak-to-peak sound pressure level of ~0.3 mbar, V = 50 m/s according to the stratospheric circulation index for this time of year and a value of R = 200 km (allowing for a small source altitude above the surface). Using these values and the conversion of 620 tonnes for high-explosive (HE) charges to be equivalent to 1 kt for a nuclear source, we find that W = 0.375 kt or $W = 1.57 \times 10^{12}$ J.

Acoustic Efficiency Approach

Following Cox (1958), the source energy is found on the basis of an equation connecting acoustic energy to the source energy through an acoustic efficient factor, ε_{ac}, for blast wave sources (Astapovich, 1946; Few, 1969; Revelle, 1980), which has previously been reported to be in the range 0.01–0.1% of the initial kinetic energy of the blast. A reevaluation of the available infrasound events from the Air Force Technical Applications Centre (AFTAC) network (Revelle and Whitaker, 1996) suggests that the actual efficiency is of order a few percent for most events. The two relations for the acoustic energy which we will interrelate are (neglecting unknown focusing and reflection factors):

$$E_{ac} = \varepsilon_{ac}\left\{\frac{W}{2\pi}\right\}R^{-2} \qquad \text{Eq. (6)}$$

$$E_{ac} = \int_0^{\tau_d} \frac{\Delta P_{o-p}^2}{\rho c_s}\,dt \qquad \text{Eq. (7)}$$

where t is time, τ_d is acoustic signal duration, ΔP_{o-p} is the positive signal amplitude (~$\Delta P_{p-p}/2$), ρ is the air density at the observation level and c_s is the adiabatic sound speed at the observation level.

To further simplify the above integral, we use the fact that for impulsive signals, we may write $\Delta P^2{}_{o-p} = \Delta P^{2/3}{}_{o-p\,\max}$. Using ρ = 1.225 kg m^{-3}, c_s = 340 m/s, R = 2 × 10^5 m, τ_d = 4 s, $\Delta P_{o-p\,\max}$ = 15 Pa (= 0.15 mbar) and ε_{ac} = 0.01, we can equate Eqs. (6) and (7) to determine W. In this way, W is about equal to 1 kt, which is in moderate agreement with the earlier empirical estimates. Note also that the factor of 2π is strictly applicable only for a certain type of meteorological setting, namely an inversion level near the Earth's surface (Cox, 1958). At 20:00 local time in the summer, however, the boundary layer conditions are probably significantly varied.

Line Source Model

Using the model of Revelle (1976) in treating the source blast as a line-source and assuming negligible energy absorption, we are able to manipulate his equations (11), (25) and (33) to derive an expression for ΔP_{o-p} in the acoustic, weak shock regime at a sufficiently large distance ($>>R_o$) from the source such that:

$$\Delta P_{o-p} = 0.2917\sqrt{p_g p_z}\left(\frac{R}{R_o}\right)^{3/4} \qquad \text{Eq. (8)}$$

where p_g and p_z are ground pressure and pressure at the source altitude, respectively, R_o is the line source blast wave radius and R is the distance from observer to source. Following Revelle (1976), the definition of a line source blast radius is R_o = (drag force on meteoroid/ambient pressure)$^{1/2}$, and using $0.5\rho V^2 A C_d$ as the drag force, it can be shown that $R_o = Md_m$ where M is the meteoroid Mach number and d_m is the meteoroid diameter. Hence, we may solve Eq. (8) for R_o and equate these expressions to yield:

$$R_o = 5.169R\left(\frac{\Delta P_{o-p}}{\sqrt{p_g p_z}}\right)^{4/3} = Md_m \qquad \text{Eq. (9)}$$

From this expression, we may compute the meteoroid diameter and, hence, its kinetic energy as we know velocity to yield:

$$Ke = 11.5\pi\rho_m R^3\left(\frac{\Delta P_{o-p}}{\sqrt{p_g p_z}}\right)^4 C_s^3 V^{-1} \qquad \text{Eq. (10)}$$

where ρ_m is the meteoroid bulk density.

Taking the source altitude to be 5 km, as previously, produces an energy yield of 0.001 kt, while adoption of a more realistic source height of 30 km based on the observations produces an energy yield of 0.64 kt.

To be more certain of any of the above estimates, we need direct recordings of the acoustic signals from the meteorite fall, which unfortunately are unavailable. These probable source energy estimates are meaningful to one order of magnitude only, though they show remarkably good internal consistency.

Seismic Data

The city of Montreal was <25 km ground distance from the fireball path. Loud detonations were heard throughout the region, rattling windows and causing skyscrapers to sway. These detonations were initially reported in the local media to have resulted in an earthquake measuring 3.8 on the Richter scale, but subsequent investigation of local seismic stations has shown that this initial report is erroneous.

The Montreal seismograph station (MNT), located at λ = –73° 37'23", φ = 45°30'09", was ~58 km ground distance southwest of the terminal point and 28 km northwest of the closest point on the ground trajectory of the fireball. Taking a nominal sound velocity in air of 0.33 km/s implies a signal travel time of 207 s from the location of the fireball detonation at 36 km altitude (total distance of 68 km). Adding this delay to the time of the detonation determined from the optical satellite data, we derive a theoretical arrival time for the airwave at MNT of 00:05:54 UT. It is important to note that signal delay speeds can vary significantly (from 0.29 km/s to 0.34 km/s for our conditions) and that this range of possible sound velocities translates into possible signal arrival times from 00:05:49–00:06:24 UTC.

The MNT was part of the Eastern Canada Telemetered Network (ECTN) operated by the Geological Survey of Canada and was digitally triggered. In this manner, any event exceeding some preset level detected by any of the 15 seismic stations comprising the network automatically triggers all other stations into recording. The MNT was a conventional short-period vertical seismograph with a useful passband between 0.5–20 Hz. All data are digitizied with a sampling frequency of 60×/s.

Near the time of the meteorite fall, no triggers occurred on MNT, attesting to the very poor coupling between the airwave and the ground near the station. Other coincidental triggers occurred at other ECTN stations at 23:56:23 UT (90 s duration) (June 14), 00:03:45

(132 s duration), and 00:10:09 (100 s duration) UTC, none related to the fireball. The expected time for the arrival of the sonic boom occurs just near the end of the second triggered datafile at MNT.

The raw unfiltered trace from MNT had a high noise level typical of seismic stations in large urban areas and showed no obvious disturbances. Subsequent filtering revealed two distinct low-amplitude seismic events on the trace. The first event is most visible in the frequency band 1–2 Hz commencing at 00:04:57 UT. It consists of a low-amplitude modulated wavetrain that persists until the end of the datafile. Similar low-frequency events are not seen on MNT at other times, nor on other stations of the network at this time, which indicates that this event represents some unusual disturbance unique to the MNT station.

The second event occurs at 00:05:55 UTC near the end of the datafile and is best seen with an 8 Hz highpass filter. A distinct increase in the energy of the wavetrain at 10 Hz can be seen as well, but the duration cannot be determined as the event is truncated by the ending of the datafile just 2 s after it begins. Similar high-frequency events are not visible on the next two closest stations of the ECTN located at distances of 133 km and 192 km from the fireball endpoint at the expected times of arrival for sonic booms. The seismic trace from MNT including these events is shown in Fig. 3.

The coincidence of the start of the second event on MNT with the expected arrival time for airwaves from the detonation of the fireball suggests that this seismic event may represent coupling of the airwave from the fireball to the ground at MNT. That this signal is primarily at high frequencies is consistent with other recorded airwave coupled signals from fireballs detected by seismic stations, such as that given by Qamar (1995) who reports that a fireball detonation at 30 km altitude recorded by multiple seismic stations showed a signal in the 8–12 Hz range. The seismic disturbance for the second event is weak, however, and the frequency characteristics are not unlike those generated by transportation and industrial

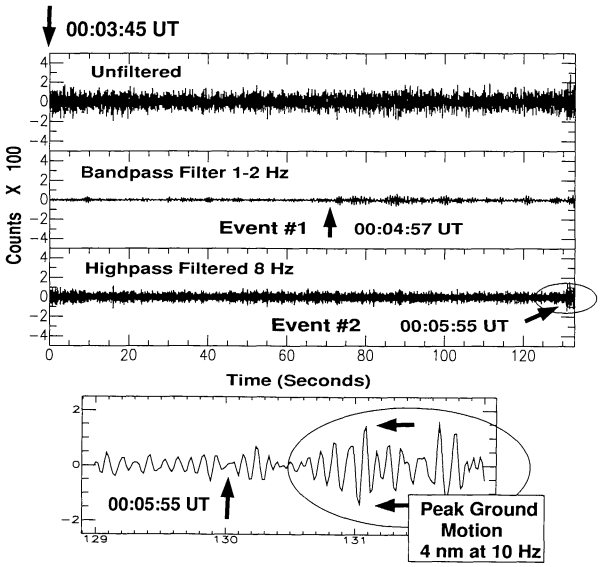

FIG. 3. Seismic data from the Montreal seismograph station (MNT). The top three graphs show the digital output from the station beginning at 00:03:45 UTC in different bandpasses. The location of the two events discussed in the text are also shown. The smaller lower graph shows an enlarged view of the second event, which may be the airwave signal from the detonation of the fireball. The arrival time for waves with velocity 0.33 km/s is also shown (00:05:55 UTC). The axes of the enlarged graph are the same as the top graphs with the ordinate proportional to ground motion

sources in Montreal. Since no other station recorded signals from the fireball, we are unable to definitively link this seismic event to the fireball.

The peak ground displacement for the second event is 4 nm at 10 Hz. This is equivalent to the motion from a Richter magnitude 0.6 earthquake at a distance of 58 km corresponding to an energy release of 10^4 J. In contrast, the total energy of the fireball ($\sim 10^{11}$ J) would correspond to a Richter magnitude 4 earthquake, thus emphasizing the weak coupling of the airwave to the ground in Montreal for the fireball which produced the St-Robert meteorite fall.

THE PROBABLE ORBIT AND ENTRY VELOCITY

From the foregoing analysis of the fireball observations, we have established most of the physical parameters needed to compute a likely orbit for the St-Robert meteoroid. The one missing datum is an initial entry velocity.

In past visual analyses of meteorite-producing fireballs, the duration of the event was used in conjunction with the established ground path to yield a velocity (*cf.*, Krinov, 1960). In many cases, however, this technique has yielded orbits incompatible with our current knowledge of meteorite orbits. It is clear that visual duration estimates cannot be reliably used to establish accurately a preatmospheric velocity.

To determine the entry velocity for St-Robert, we appeal to the abundance of data that have been gathered by the major fireball camera networks, particularly the Prairie Network (PN; *cf.*, McCrosky *et al.*, 1976) and the Meteorite Observation and Recovery Project (MORP; *cf.*, Halliday *et al.*, 1978). By utilizing the large number of fireballs detected by these networks believed to be associated with meteorites, we can define a range of orbital parameters for a meteorite orbit consistent with fireball network data. In particular, the value for the aphelion distance of orbits for meteorite-producing meteoroids is constrained to be inside the orbit of Jupiter, with a large fraction also having aphelion beyond the orbit of Mars. Halliday *et al.* (1989a) found only 4 meteorite-producing fireballs from a total of 44 from MORP that had aphelia inside the orbit of Mars, while Wetherill and Revelle (1981) who analyzed 27 PN fireballs believed to be of chondritic composition also found 4. Considering other uncertainties in our analysis and the fact that all 4 recovered meteorite specimens with accurately determined orbits have aphelia in the main asteroid belt, we feel justified to require that our assumed orbit have an aphelion between Mars and Jupiter, just as required by the bulk of the camera network data. A similar method has been used by Halliday and McIntosh (1990) to determine the probable orbit for the Murchison meteorite and by Griffin *et al.* (1992) for the Abee meteorite. We can then use the observed mean velocity derived from the IR observations between 37–33 km altitude in combination with a theoretical model of the breakup and deceleration of the meteoroid to refine our initial velocity range and so better determine the orbit.

To derive an initial range of orbits for St-Robert, we chose a combination of azimuths and altitudes for the apparent radiant that were compatible with the range of errors associated with the trajectory of the fireball, in conjunction with assumed velocities of 12–17 km/s. As the slope for the trajectory was poorly constrained by visual observations, we make use of the IR slope of 58° assuming a probable error of 3° and the visually determined azimuth of the trajectory of 202° ± 5°. Possible orbits were calculated with variations in steps of 1° in azimuth and altitude and 0.1 km/s in velocity resulting in a total of 3850 possible orbits for the assumed

TABLE 1. Representative possible orbits for the St-Robert meteorite. Symbol definitions are given in the text.

At	55	55	58	59	58*
Az	197	201	204	206	202
V	13.5	13.0	14.0	13.2	13.0
α_r	179	176	175	174	176
δ_r	3	2	9	9	6
a	2.3	1.9	2.7	2.1	1.9
e	0.56	0.48	0.63	0.51	0.48
ι	0.4	0.0	1.3	1.0	0.7
ω	182	0.0	179	178	179
Ω	83.764	263.764	83.764	83.764	83.764
q	1.0156	1.0158	1.0157	1.0155	1.0158
Q	3.54	2.86	4.39	3.08	2.86
ε	5	2	6	6	4

* The most probable orbit is shown in the last column.

range in fireball-trajectory values. Approximately one-half of these orbits met our acceptance criterion of having aphelion between Mars and Jupiter.

A representative sample of several possible orbital solutions is given in Table 1 along with the "best-fit" solution for V = 13 km/s. Here *At* is the assumed altitude of the radiant in degrees, *Az* is the assumed azimuth and *V* is the preatmospheric velocity. The remaining columns in the table include the right ascension (α_r) and declination (δ_r) of the radiant, corrected for the Earth's gravitation and rotation; semi-major axis (*a*) of the orbit in Astronomical Units (AU); orbital eccentricity (*e*); orbital inclination (*i*); argument of perihelion (ω); longitude of the ascending node (Ω); perihelion distance (*q*); aphelion distance (*Q*); and the angular distance from the radiant to the antapex in heliocentric coordinates (ε). The angular values α_r, δ_r, *i*, ω, Ω are given in degrees and refer to equinox 2000.0.

Table 2 presents the range of values for the orbital elements and also a mean and standard deviation for the sample chosen. Given the artificial nature of the intervals chosen for the three free parameters (entry velocity, azimuth and altitude of the radiant), the mean and standard deviation have little real meaning. We present them here simply to provide a feeling for the distributions involved. The range of values has more physical significance.

It is immediately obvious that the initial velocity is quite tightly constrained near a value of 13 km/s with an error of ~1.3 km/s. No orbital solutions fitting our criteria are possible for entry velocities in excess of 14.3 km/s. The range of values for *e* and *a* reflects the constraint we have placed on *Q* and the further constraint that the meteoroid be Earth-intersecting. The inclination lies between 0° and 2.2° with a most probable value near 0.7°, which is somewhat lower than the mean values of 7.7° and 8.2° found by the PN and MORP (Halliday, 1983) but similar to the inclination distribution of the main-belt asteroids near the 3:1 mean-motion resonance where dynamical studies suggest the chondrites originate (*cf.*, Wetherill and Chapman, 1988). The longitude of the ascending node is defined by the time of observation of the fireball and for most potential orbits indicates that the collision with Earth occurred at the descending node, though an ascending node collision is not strictly ruled out. The elongation of the radiant from the antapex direction in heliocentric coordinates is quite small, as is the case for most meteorite radiants (Levin and Simonenko, 1969). The effect of this geometry is to limit strongly the possible range of perihelia to very nearly the value for the Earth's distance from the Sun at the time of fall (r_{earth} = 1.0158 A.U.). The tendency of the perihelion distance for the orbits of chondrites to occur near the Earth is a characteristic feature of such orbits (*cf.*, Wetherill, 1968; Wetherill and Chapman, 1988) resulting from their short dynamical evolution and atmospheric survival biases.

TABLE 2. Mean values, standard error and range for the ensemble of possible orbits for the St-Robert meteoroid.

	Mean	Std. Dev.	Range
At	57.5	1.7	55–60
Az	202	3	197–207
V	13.1	0.7	12–14.3
α_r	176	2	171–180
δ_r	-5	3	–4–12
a	2.1	0.4	1.43–3.0
e	0.5	0.1	0.29–0.66
ι	0.7	0.5	0–2.2
ω	–	–	358–2, 178–182
Ω	–	–	263.764, 83.764
q	1.0157	0.0001	1.0154–1.0158
Q	3.11	0.88	1.84–5.0
ε	5	2	0–10

The range has the most significance; the mean and error are indicative of the spread in values within the sample.

We note that modest changes in the assumed altitude and azimuth of the radiant beyond the error limits adopted do not change the essential features of the probable orbit nor affect the possible entry velocity.

THEORETICAL MODEL OF ENTRY

In an effort to reconstruct further the initial velocity and initial mass for St-Robert from observations, we have employed a model of meteoroid entry incorporating fragmentation, the details of which

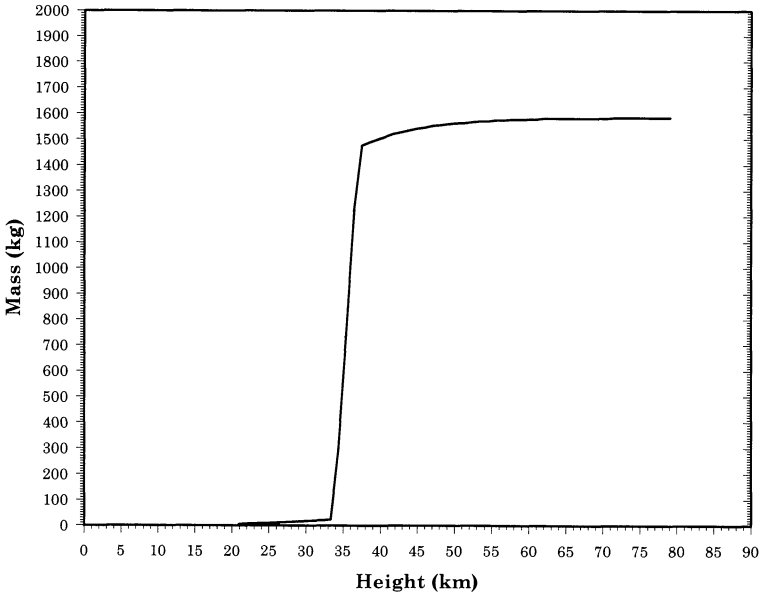

FIG. 4. The theoretical mass loss as a function of height from the fragmentation model. Fragmentation begins at 37 km altitude and lasts for 0.4 s before ceasing at 33 km altitude. The final mass is equal to the mass of the largest recovered fragment (6.5 kg).

are presented by Ceplecha *et al.* (1993). This model follows the classic single-body treatment with the incorporation of one or more points of gross fragmentation along the trajectory.

By using the entry slope determined from the IR observations, the stipulation that the velocity of the largest fragment be close to the 12.2 km/s mean velocity found for the debris cloud over the height interval 37–33 km from the IR satellite data, and constraining the equivalent luminosity of the resulting fragmentation to be in accordance with that observed by the optical satellite sensors in both magnitude and duration, we have attempted to reconstruct the most probable entry conditions for the St-Robert meteoroid. It is important to note that uncertainties in the actual peak magnitude for St-Robert due to the assumption of a 6000 K blackbody model for emission, lack of instrumental observations earlier in the trajectory and smaller errors in estimated luminous efficiency for such a large body make the final result somewhat uncertain.

In modeling the light curve, we have employed the revision of the luminous efficiency scale recently computed by Ceplecha (1996) from Lost City to 5.2%, which is in good agreement with the estimate for Innisfree (~4–8%) found by Halliday *et al.* (1981), together with the functional dependence on velocity taken to be in accordance with the results of Ayers *et al.* (1970). We have also assumed that the ablation coefficient, σ, is 0.02 s^2 km^{-2} at all times, which is in accordance with the average value found for fireballs believed to have produced meteorites (Wetherill and Revelle, 1981).

Figure 4 shows the "best-fit" mass loss as a function of height. From this, we compute a theoretical initial mass of ~1600 kg. This is the mass needed to produce the optical light curve, to match observed IR velocity in the 37–33 km height range (for an initial velocity of 13 km/s) and also become subluminous (<4 km/s) with the largest remaining mass equal to 6.5 kg (the largest found in the strewn field). Figures 5 and 6 show the theoretical light curve as a function of time and also the velocity as a function of height.

The initial mass estimate may be slightly lower for a higher initial velocity of ~14 km/s (possibly as low as 1400 kg) and could be somewhat larger for a lower initial velocity of ~12.5 km/s (approaching 2000 kg). As the latter is the more likely given the low velocity observed in the IR in the 37–33 km range, we believe an entry velocity in the 12.7–13.3 km/s range to be most probable according to this theoretical model. If fragmentation occurred earlier in the trajectory, the initial mass could be even larger than this 2000 kg estimate. It is useful to note that the dynamic pressure at the point of major fragmentation at 37 km altitude was 9×10^5 Pa, which is a value similar to Lost City at its first fragmentation point (6×10^5 Pa) (Ceplecha, 1996).

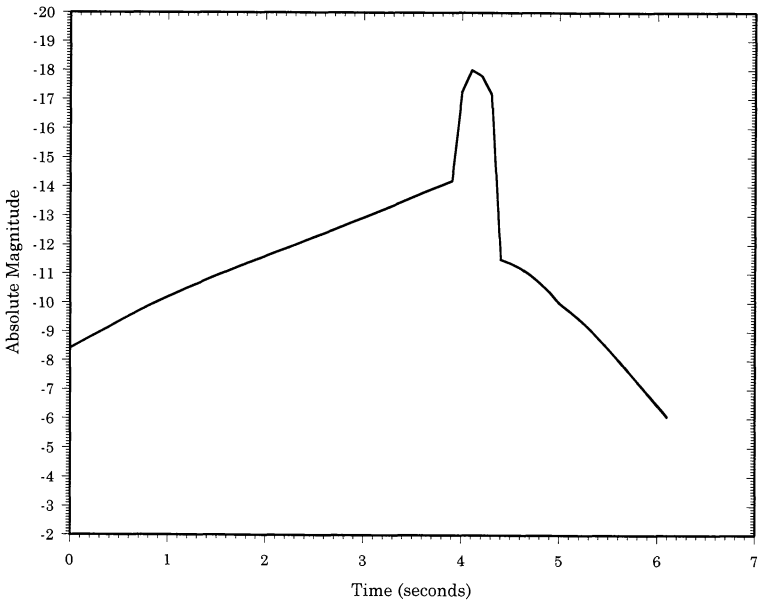

FIG. 5. Equivalent visual light curve from the theoretical model.

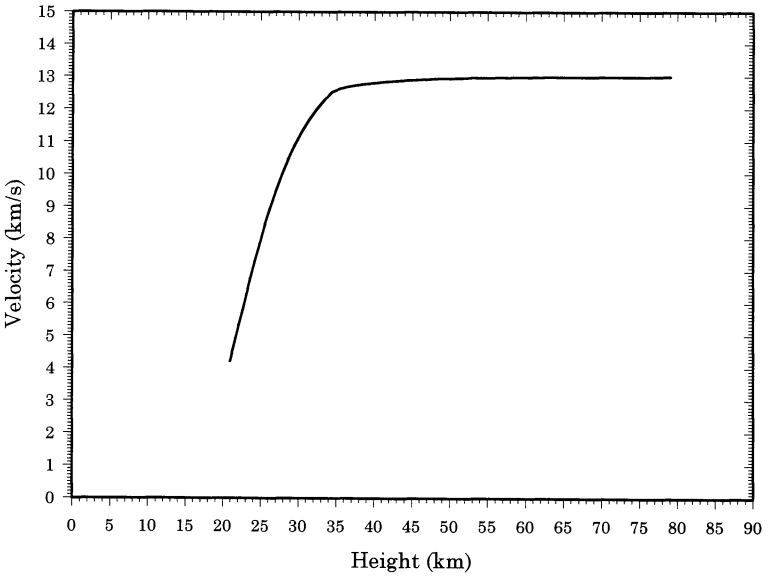

FIG. 6. Effective velocity as a function of altitude for the largest mass associated with the St-Robert meteoroid derived from the theoretical model.

THE FALL ELLIPSE AND IMPACT PHENOMENA

The distribution of the 20 recovered meteorite fragments in the region near St-Robert ($\lambda = -73°00'04"$, $\varphi = 45°58'19"$) is shown in Fig. 7. Related details for each fragment are given in Table 3. The fall region is located on the St. Lawrence lowlands, a favored agricultural area, so that three-quarters of the fall ellipse are grain and corn fields or cow pastures. Parts of the west and southwest regions of the ellipse are forested.

In most cases, meteorite fragments were recovered by local residents alerted to the possible presence of such material by active canvassing or through media reports. Organized field searches including some of the authors (AH, DP, and PB) accounted for recovery of 10 fragments. One fragment near the southwest corner (uprange portion) of the ellipse hit the aluminum roof of a shed and left a noticeable depression before rolling off the roof (Fig. 8). Three meteorite fragments were found on roads or paths and three on lawns, all of the latter were within 20 m of houses.

The four largest fragments left sizeable plunge pits. Unfortunately, excavation by finders destroyed information on the pits with the exception of the first recovered fragment of 2.3 kg, whose

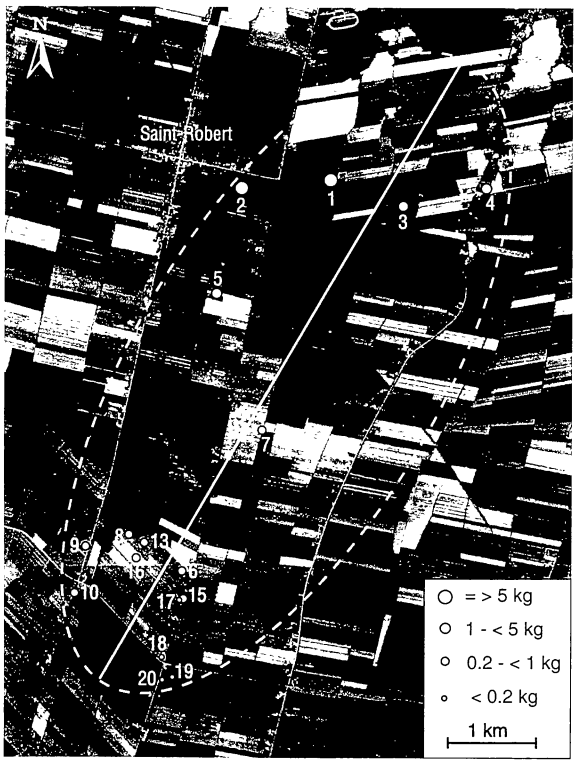

FIG. 7 (left). Corrected aerial photo mosaic (constructed from aerial photographs taken 1984 August 22) for the St-Robert meteorite strewn field. Locations of individual fragments are shown as dots and are numbered following Table 3. The ellipse of fall is oriented at 210° ± 10° and its dimensions are 8 × 3.5 km. Most of the region is farmed, only the darkest gray areas are forested.

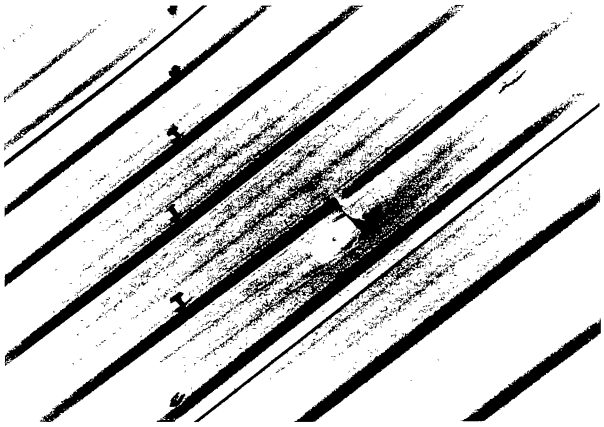

FIG. 8 (above). Impact damage to aluminum shed roof due to the fall of fragment 18.

TABLE 3. Details for individual fragments recovered from the St-Robert fall. Where available accurately, the location and date of recovery of the specimen are given.

Number	Date	Mass (g)	Latitude	Longitude	Comments
1	06 17 94	6552	45°58'07"	72°58'41"	In pit–chipped on impact.
2	06 16 94	5438	45°58'07"	72°59'24"	Found in pit.
3	09 13 94	3708	45°58'02"	72°58'03"	Found in pit three months after fall; weathered and muddy.
4	06 14 94	2297	45°58'08"	72°57'19"	Chipped in pit.
5	06 22 94	1500.7	45°57'31"	72°59'46"	Penetrated deeply–pit diameter ~35cm. Angular.
6	06 20 94	755	45°55'56"	73°00'04"	Found on path; 6 cm pit.
7	06 22 94	701	45°56'40"	72°59'21"	Found on road–chipped by lawnmower?
8	06 23 94	644	45°56'00"	73°00'30"	Pit?
9	06 20 94	598	45°55'53"	73°00'55"	Hit lawn; oriented specimen.
10	06 23 94	533	45°55'38"	73°01'09"	Found 12cm from paved road.
11		516.96			Embedded in ground–broken in two.
12		459.12			Embedded.
13		442.88	45°55'55"	73°00'27"	In pit; cut nearby pine needles during descent.
14		323.6			Embedded?
15	06 26 94	290.44	45°55'35"	73°00'06"	Embedded in lawn.
16	07 30 94	253.75	45°56'19"	73°00'31"	Buried to 10 cm depth.
17	07 23 94	158.5	45°55'34"	73°00'07"	Chipped and buried in lawn.
18	06 15 94	80.52	45°55'14"	73°00'18"	Hit roof of shed–chipped.
19	06 25 94	75.64	45°55'05"	73°00'18"	Embedded in ground.
20	06 25 94	54.68	45°55'07"	73°00'13"	About one-quarter of broken individual.
1a	06 20 94	19.9	45°58'07"	72°58'41"	Endpiece from no. 1.
1b	06 17 94	9.1	45°58'07"	72°58'41"	Chip from no. 1.
17a		0.23	45°55'35"	73°00'06"	Chip from no. 17.

plunge pit was partially preserved (Fig. 9). Measurement of this pit revealed that it was oriented toward azimuth 200° ± 10°, with a depression angle from the horizontal of 65° ± 5°. The hole was ~15 cm in diameter and 20 cm deep. The terminal velocity for a fragment of this mass is ~50 m/s, which is consistent with the size of the depression. It is not known why this pit showed a sizeable orientation, as a fragment of this size is expected to be falling within a few degrees of the vertical near the ground. A strong tail wind near the ground or significant lift forces (Passey and Melosh, 1980) may be possible explanations. Fragment 13, which was found in a 10 cm deep pit in a red pine forest, had sliced cleanly through several branches cutting a half-moon in the 8 cm long pine needles on one branch. The alignment of the trimmed branches and the pit established an approach from 31° azimuth with a dip of 78°. This very different landing trajectory suggests that "flying" by individual pieces may have been a substantial agent in determining fall locations for individual fragments.

The soft soil, particularly in plowed areas, allowed pit formation by several of the smaller fragments. In some cases, fragments as small as 250 g were completely buried under the surface. Recognition of this "burying" phenomenon and the fact that there are almost no natural stones in these fields led searchers to adopt a method of using ski poles to probe small holes in fields for the presence of meteoritic material; a total of five fragments were found in this manner.

Several witness reports in the region suggest that the fall of material was greater than is presently known. One report to the southwest of the fall ellipse mentioned that fine, dark-colored dust

FIG. 9. Plunge pit associated with fragment 4.

was present on cars and objects shortly after the fall, but this could not be confirmed. Such dust falls are known to have been associated with the fragmentation of other large, chondritic masses in the atmosphere (*cf.*, Folinsbee and Bayrock, 1961; Nininger, 1952).

Several witnesses gave accounts of fragments falling nearby. Perhaps the most spectacular is that of Mr. and Mrs. Claude Proulx, who were relaxing on their patio near the uprange portion of the fall ellipse when the event occurred. After hearing the detonation and seeing the dust cloud, the couple heard a whistling sound toward the north, followed by the sound of an object falling somewhere through leaves on nearby trees. Immediately after this, another whistling sound followed by a "thud" was heard to the northwest and almost simultaneously another whistling sound and "thud" to the east. Proulx was left with the impression that his neighbor to the south was pelting golf balls at him. Extensive searching of the immediate area did not produce any fragments.

Another resident of the area, Denis Racine, was outside mowing grass ~2 km south of the uprange portion of the ellipse when the fireball occurred. After hearing the loud detonation over the sound of the mower, he looked up to see the dust cloud to his south and several "streamers" emanating from the main cloud. Racine noted at least three distinct contrails heading to his northeast and one to the northwest of his location. These may correspond to the four largest masses in the 2.3 to 6.5 kg category.

One additional account from the fall region deserves mention. Vital Lemay was working on his farm on the west side of the ellipse when the fireball occurred. He first heard 2–3 small bangs, then felt the ground shaking. Looking up, Lemay saw the dust cloud and then heard two whistling sounds, one very loud, immediately to his north, and one fainter to the south. The sound to the north ended with a low "thud." Lemay's location was 600 m south of the 5 kg fragment and 900 m north of the 1.5 kg fragment on the west side of the ellipse, and it is likely that these are the fragments responsible for the noise. Several other residents in the region of the fall ellipse reported whistling sounds as well. Similar whistling sounds near the fall points of other meteorites have been reported extensively in the literature (*cf.*, Nininger, 1952; McCrosky *et al.*, 1971).

DARK FLIGHT

In an effort to provide a link between the visual and satellite IR observed trajectory/detonation point with the meteorite strewn-field pattern, we have attempted to model the darkflight portion of the meteorite fall. The wind pattern at upper altitudes is critical in determining the final impact point for smaller-sized (less than a few kilograms) fragments (*cf.*, McCrosky *et al.*, 1971; Halliday, 1985).

TABLE 4. Observed upper wind data for the region near St-Robert at the time of fall.

Pressure (Pa)	Height (km)	Temp. (°C)	Wind Dir.*	Wind Speed (m/s)
11.7	30.461	–40.2	053	10.3
13.8	29.337	–41.1	057	9.7
15.0	28.775	–43.7	077	10.3
15.9	28.383	–45.5	092	11.2
20.0	26.861	–47.6	099	14.9
23.1	25.918	–51.6	110	13.4
25.0	25.408	–52.4	106	12.3
30.0	24.233	–54.4	074	9.8
40.0	22.390	–54.2	050	6.2
42.7	21.972	–54.2	055	5.1
47.8	21.253	–57.0	061	5.7
50.0	20.938	–56.1	012	3.0
100.0	16.585	–61.8	311	11.0
200.0	12.316	–56.5	316	32.0
300.0	9.626	–35.0	286	17.0
400.0	7.544	–17.8	289	7.0
500.0	5.814	–7.4	295	12.0
600.0	4.401	1.5	283	10.0
700.0	3.146	8.2	269	3.0
800.0	2.036	11.7	234	5.0
900.0	1.045	13.7	013	2.0
950.0	0.585	18.2	054	5.0

*Wind Dir. is the azimuthal direction (in degrees measured positive east of north) from which the wind appears to be blowing. The data <20 km altitude are taken from Maniwaki radiosonde measurements made at 0 UT June 15 while those >20 km are from Buffalo, New York, radiosonde data made at 23 UT June 14.

Upper-wind data from radiosonde measurements taken in Maniwaki (~200 km due west of St-Robert) at 0h UT on June 15 are shown in Table 4. Since the Maniwaki data do not go above 20 km altitude, all higher wind data were taken from measurements made in Buffalo, New York <1 h earlier. Errors in the fireball trajectory and drag coefficients are much more important than the error incurred by having upper wind data from a location a few hundred kilometers from the fall ellipse.

The most important feature to note from Table 4 is the west wind blowing across the fireball path at most altitudes at the time of the fall. As a result, smaller fragments were probably blown proportionately farther east off the IR nominal trajectory so that the fall ellipse major axis would tend to rotate toward the down wind direction, pivoting about the larger masses. The main axis of the ellipse is oriented along azimuth ~210° (Fig. 7), while the fireball trajectory has an azimuth of 202°, the difference being opposite to that expected for wind effects. The ellipse determined from the recovered meteorites, however, is not the complete ellipse as there is almost certainly a negative bias in recovery probabilities in the western portion of the strewn field due to forest and this explains the discrepancy.

To model the fall, we have assumed that the velocity of fragments as they become subluminous is 4 km/s, which is a value similar to those found for other meteorite-producing fireballs near the end of luminous flight (McCrosky *et al.*, 1971; Halliday *et al.* 1981). Variations of 1 km/s in the assumed velocity at the end of the luminous path produce very similar results. The drag coefficients used for the darkflight model were those of a hemisphere

appropriate to the different flow regimes encountered by the rapidly decelerating body, where the hemisphere has a low-velocity (subsonic) drag coefficient of ~1.1.

Our instrumental atmospheric entry slope of 58° for the visible fireball was used throughout. Since most of the smaller masses assume nearly-vertical flight a few seconds after passing the visible fireball's terminal height, increases in the slope above this value produce little change in the final impact point. Much shallower atmospheric slopes (*e.g.*, near 10°) can alter the final distribution significantly, but the observations do not support such low-angle trajectories for the fireball. Changes in the assumed azimuth of the radiant, that are somewhat beyond the error values derived from the visual observations, do not significantly alter the final relative distribution of meteorite fragments as the cross-wind perturbation is the dominant effect.

The parameter upon which the final ground distance from the terminal point depends most sensitively is the assumed height of the luminous terminal point. To demonstrate this, Fig. 10 shows the apparent impact positions for 10 mass sizes as a function of distance from the terminal point for two heights. From the IR observations, fragments were still moving with significant velocities at altitudes as low as 33 km. For larger fragments, we would expect deceleration by ~25 km altitude to result in subluminous velocities if most fragmentation took place in the 37–33 km height range. As a result, we show the spread expected for each mass category from the subluminous point for 33 km altitude and 25 km altitude.

Although this assumes that all masses separate at one specific height, which is almost certainly not the case, it does place useful constraints on the end height if we stipulate that most of the fragmentation was confined to a relatively short (~5 km) length of the trajectory near the end height, which is an assumption supported by the satellite data. If smaller fragments were released substantially higher in the atmosphere than the large fragments, we should expect these to be further to the east of the fireball ground-path, and in some cases further along the ellipse, than larger fragments depending on surface area/mass ratios. This is not the observed pattern, which shows a remarkably regular gradation of masses from south to north along the major axis of the fall ellipse, suggesting a narrow height range for the main breakup. The major axis of the observed ellipse agrees with the best estimate for the azimuth of the ground path to <10°, thus reaffirming the internal consistency of the derived quantities. Considering that the darkflight does not take into account lift forces that may be present or nonhemispherical drag coefficients, the agreement is encouraging.

From the estimated height of breakup and using the theoretical modeling for the final portion of the fireball trajectory, it is expected that the largest fragments will move ~10 km along the ground from the fragmentation point to the terminal point, with smaller fragments moving some distance less than this value, but beginning their darkflight at higher altitudes. By adding the final darkflight distances as shown in Fig. 10, we may compute the total distance traveled from the detonation point to the ground point. For the largest masses, this will be a distance of ~15 km, placing the ground-point of the detonation <2 km from the middle of the error box for the detonation point on the ground determined by the visual observations and within 6 km of the point determined by the IR observations. All of these values are within the error margins for both the visual and IR observations, particularly when one considers that the 0.5 s duration of the breakup as evidenced from both the IR and optical satellite sensors implies a distance of ~5 km on the ground for the region of breakup as opposed to an idealized "point."

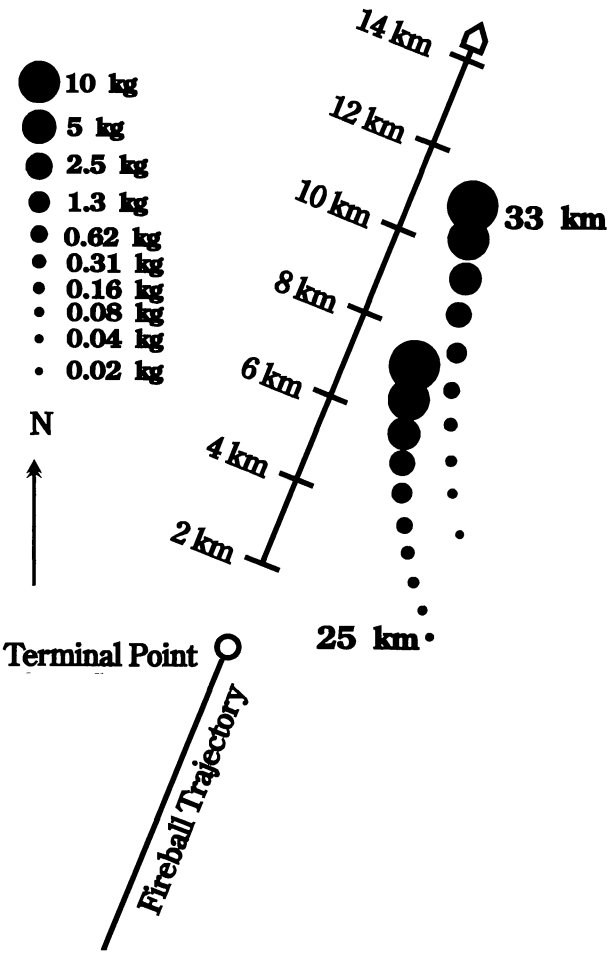

FIG. 10. Computed ground point for ten mass sizes, with two assumed detonation heights. The ground point shown and the major axis with linear scale points in the direction of travel for the fireball (202°).

METEORITES AND TOTAL FALL MASS

St-Robert has been typed as an H5 with slightly brecciated texture (Wilson, 1994). Most of the fragments have a complete fusion crust. Fragment 5 has an unusual angular shape and shows at least two separate fusion-crust ages, which suggests that it was involved in multiple fragmentations before becoming subluminous. Fragment 3 has an irregular surface with one protruding planar surface indicating preentry fractures in the meteoroid. Fragment 9 is highly rounded and shows frothing on its capped-end indicating that it had been oriented in flight (*i.e.*, was not rotating); this is the only obviously oriented fragment of the 20, a proportion similar to that found for other meteorite showers (Nininger, 1952). Flow lines are present on several of the specimens. In two cases, the individuals had been broken (fragments 11 and 20) after ablation had ceased. These two fragments were not broken from ground contact, although several other pieces showed minor chipping from ground contact as evidenced by the damage being limited to the down side with the recovery of the chips adjacent. The fragment that struck the roof was the most severely chipped individual, and one other piece had apparently been damaged by a lawn mower. The cause of the breakage of these two fragments during their dark flight is unknown, and the mating pieces were not found.

Table 3 lists a total recovered mass of 25.411 kg. A likely second plunge pit near the location of the 2.3 kg piece was located more than a week after the fall, and it appears probable that a ~5 kg fragment was removed but not included in this tally. The total recovered mass therefore may be ~30 kg. The question of larger pieces remaining unfound is open, although the region further to the northeast of the ellipse is almost completely unforested and mostly pasture, making discovery of any such large masses somewhat likely. An aerial search by one of the authors (AH) with a fixed wing aircraft at 200 m above ground level of the area to the northeast of the ellipse failed to locate any additional plunge pits.

The Mbale meteorite shower of 1992 (Jenniskens *et al.*, 1994) produced a large number of documented fragments that followed a power-law mass distribution. Indeed, most fragmentation phenomena follow power-law distributions, with the majority of the mass being contained in the larger fragments (Fujiwara *et al.*, 1989). Following Jenniskens *et al.* (1994), we have put the 20 fragments by mass in bins, each bin 2.5× larger in mean mass than the preceding one (*i.e.*, 1/4 decade in size) beginning with the smallest recovered individual. Jenniskens *et al.* (1994) showed that the Mbale mass distribution followed the relation

$$dN(m)m \sim m^{k/3}d(\log(m)) \qquad \text{Eq. (11)}$$

where m is mass, $N(m)$ is the number of fragments with mass m and k is a constant characteristic of the fragmentation process. The value k = 1.2 was derived by Fujiwara *et al.* (1989) for fragment diameters more than about one-tenth that of the initial body (or 0.001 that of the initial mass M_i); for smaller sizes, k = 0.6. Figure 11 shows the total mass as a function of the mass interval. The least-squares fit to the line is also shown and the associated total mass for this fit is 25 kg, as expected from the total mass recovered on the ground. Assuming that all fragments >5 kg have been recovered, we have extrapolated the appropriate power-law fits found by Jenniskens and introduce a "knee" for the discontinuity for fragments near 1.5 kg, which are representative of the bin closest to the 10^{-3} M_i value. The total mass in this distribution is 51 kg. The uncertainty concerning the existence of a large mass associated with the plunge pit found near fragment 4 results in a formal uncertainty in the final mass of ~20 kg. Our best estimate for the total mass reaching the ground using this method is 51–71 kg.

The total fall mass may also be estimated from the number of fragments recovered in the uprange portion of the fall ellipse where areas of known size were searched. (Using the Universal Transverse Mercator, UTM, 1 km grid squares as a randomly imposed grid, this area encompasses 9 km^2.) For example, one meteorite was recovered from a depression on the shoulder of a road in this area. The roads are 10 m wide; three roads cross the area so that the roads encompass one 1/100 of the area; therefore a total of 100 meteorites is predicted in this 9 km^2. Including yards and buildings along the roads adds two more strips (people live along only two of the roads) averaging ~10 m wide. Three meteorites were found in yards (two witnesses in this area also reported meteorites, uncounted in this calculation, falling through the trees in their yards that were never found) or after hitting buildings. We are thereby able to infer that ~450 meteorites fell in the area. Combining this with the road recovery estimate to improve population statistics yields 240 meteorites in the 9 km^2. This number compares favourably with the estimated yield from the most productive (and most searched) UTM kilometer square. Six meteorites were found in this grid square that

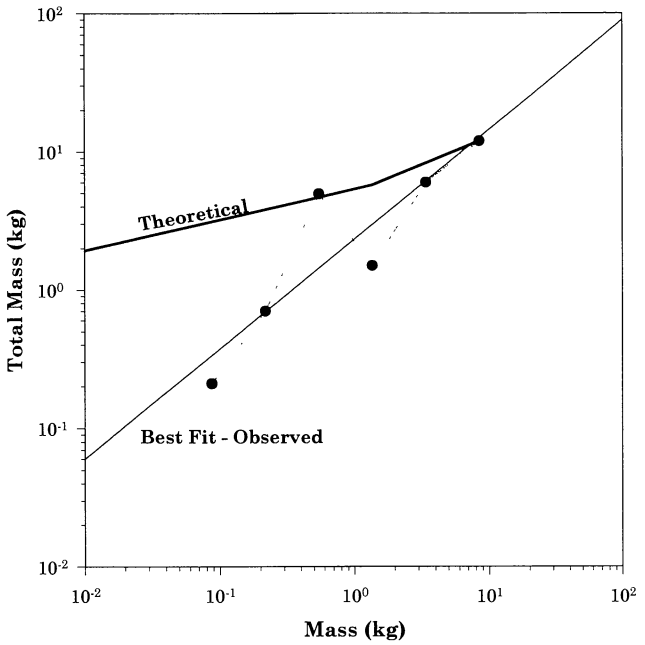

FIG. 11. Observed and theoretical mass distribution of fragments from the St-Robert meteorite shower. The theoretical curve assumes that all masses >5 kg have been found.

was approximately half searched. Adding a search efficiency of 50% to account for ground conditions (from a test of blind searching for placed meteorites) implies a yield of 216 meteorites from the 9 km^2. The average mass for the 14 recovered meteorites in this area is 370 g. Taking the 240 population estimate as most valid, this yields ~90 kg of meteorites from these 9 UTM grid squares. Using instead only the area roughly bounded by the 14 meteorite recoveries yields an area of approximately half this size and therefore ~45 kg of meteorites distributed through 120 individual fragments. So we can estimate conservatively that ~40 kg of meteorites remain undiscovered in this uprange portion of the ellipse. This sets a lower limit of ~65 kg of sizeable (≥55 g) meteorites for the fall, which is in good agreement with the size distribution estimate of 51 (+20) kg. Both estimates are most uncertain because recovery may be incomplete for the larger fragments in the remainder (downrange) portion of the ellipse. Due to this factor and to the fact that the full extent of the fall ellipse is not known, we regard our mass estimate as open upwards by a factor of 2 allowing as much as 130 kg in the St-Robert fall.

COSMOGENIC NUCLIDES AND INITIAL MASS

Cosmogenic nuclides contain valuable information that can reveal the recent history of a meteorite, on timescales ranging from the past few weeks (*e.g.*, using ^{48}V, with $t_{1/2}$ = 16 d) to the past few million years (*e.g.*, using ^{26}Al, $t_{1/2}$ = 705 ka). Such information can be used to determine cosmic-ray exposure ages, terrestrial residence times, effects due to multistage exposures, and variations in the cosmic-ray flux..

The first recovered piece of St Robert (2.287 kg) (fragment #4) was hand-carried by Dr. R. Herd to Richland, Washington. Counting began on 1995 June 17 at 5:40 P.M. (PDT), which was slightly over 72 h after the fall. This is one of the earliest counts ever of a freshly fallen meteorite. The remaining specimens were shipped in three batches. All counting was completed by 1996 March.

Samples were counted for at least one day, and others for up to five days, to measure activities of various short- and long-lived cosmogenic radionuclides. Most of the counting was done using a high-efficiency NaI(Tl) multiparameter gamma spectrometer (for assaying ^{22}Na, ^{26}Al, ^{46}Sc, ^{48}V, ^{54}Mn, ^{56}Co, and ^{60}Co). This detector uses two 30 cm diameter × 20 cm thick NaI (Tl) crystals for coincidence detection of multiple gamma rays, leading to a large reduction in background and interferences caused by other radionuclides, cosmic rays, and detector noise. Several of the samples were also counted using an anticoincidence-shielded intrinsic Ge gamma spectrometer (for assaying ^{7}Be, ^{51}Cr, ^{54}Mn, ^{57}Co, and ^{58}Co). Further details on this instrument are given by Brodzinski (1973), Perkins *et al.* (1970), Wogman *et al.* (1967 and 1970), Reeves *et al.* (1984), and Miley *et al.* (1992).

Calibration procedures for ^{26}Al were the same as used for the analysis of Antarctic meteorites (Edwards *et al.*, 1982; Evans and Reeves, 1987), which uses a calibration curve based on our extensive library of mockups of freshly fallen meteorites. For ^{22}Na and ^{60}Co, a series of mockups (10 and 4 for each isotope, respectively) were used to calibrate the instrument in a fashion similar to that used for ^{26}Al. For the other radionuclides, a combination of procedures was used. Calibration data were obtained by measuring existing mockups containing ^{22}Na and ^{60}Co and by using data from previously counted fallen meteorites measured on the same instruments. This procedure, although less accurate, avoided the expense of fabricating new mock-ups for the short-lived isotopes, as was done in the past. These procedures resulted in data accurate to 5–10% for ^{26}Al, 10–15% for ^{22}Na and ^{60}Co, and ~25% for the other isotopes, excepting those with low signal-to-noise.

The radionuclides detected in St-Robert are given in Table 5. These data are given in decays per minute per kilogram of meteorite (dpm/kg). All data have been corrected to the time of fall. In addition, ^{7}Be ($t_{1/2}$ = 53 d), ^{51}Cr ($t_{1/2}$ = 28 d), ^{57}Co ($t_{1/2}$ = 272 d), and ^{58}Co ($t_{1/2}$ = 71 d) were detected using the Ge detector. The detection of ^{24}Na in specimen #4 (^{24}Na 60 ± 15 dpm/kg) was possible due to the rapid recovery and transport of the specimen to the counting laboratory in Richland. This also permitted the detection of other short-lived radionuclides such as ^{48}V.

The ^{26}Al and ^{22}Na activities in the 14 specimens of St-Robert are somewhat on the high side for an H-chondrite, for which normal values fall near 55 ± 8 dpm/kg for ^{26}Al (Evans and Reeves, 1987) and 60–110 dpm/kg for ^{22}Na (Evans *et al.*, 1982). St-Robert fell about three years past the most recent solar maximum in 1991, during which time the ^{22}Na production rate should have been at a level intermediate between the minimum and maximum levels, while the ^{60}Co rates should have been near minimum values due to solar modulation of the galactic cosmic-ray (GCR) flux. Past results (Evans *et al.*, 1982) show that H-Chondrites that fell during the 1969 solar maximum had ^{22}Na activities in the range of 60–80 dpm/kg, whereas those falling during the 1976 solar minimum had activities in the range of 80–110 dpm/kg. Many of the St Robert ^{22}Na activities fall outside the normal range. The range in the Al and Na activities may be due in part to differences in cosmic-ray shielding, which indicates that the St-Robert specimens were scattered throughout the original preatmospheric mass. The ^{60}Co activities confirm this observation, as this isotope is more sensitive than ^{26}Al or ^{22}Na to both the mass and depth within the preatmospheric body (Eberhardt *et al.*, 1963; Michel *et al.*, 1991).

In addition, systematic differences exist in the relative activity levels of ^{26}Al, ^{22}Na and ^{60}Co when all specimens are compared. Using the model results of Bhandari *et al.* (1993) for ^{26}Al and ^{22}Na and of Spergel *et al.* (1986) for ^{60}Co as a function of depth and

TABLE 5. Cosmogenic radionuclides in St Robert (activities in decays per minute per kilogram, dpm/kg). Data are corrected to time of fall: 6/14/94 5.02 P.M. PDT. For each nuclide activity, the highest (H) and lowest (L) values for all fragments are indicated.

Sample		**#4**	**#9**	**#6**	**#20**	**#19**	**#15**	**#17**	**#16**
Mass (kg)		2.287	0.598	0.755	0.055	0.076	0.290	0.159	0.254
Analysis Date		06 17 94	06 30 94	07 16 94	09 24 94	09 25 94	09 21 94	09 23 94	09 22 94
	$t_{1/2}$								
^{60}Co	5.3 a	15.3 ± 1.5	11.9 ± 1.2	8.7 ± 0.9	15.6 ± 1.6	L3.5 ± 0.4	37.8 ± 3.8	53.1 ± 5.3	24.1 ± 2.4
^{22}Na	2.6 a	L72.8 ± 7.3	83.7 ± 8.4	74.0 ± 7.4	107.1 ± 11	100.7 ± 10	110.1 ± 11	121.1 ± 12	103.7 ± 10.4
^{26}Al	700 ka	L50.1 ± 2.5	58.7 ± 2.9	59.7 ± 3.0	70.2 ± 3.5	61.0 ± 3.0	H83.4 ± 4.2	70.9 ± 3.5	67.7 ± 3.4
^{54}Mn	312 d	129.2 ± 32	134.3 ± 34	L119.0 ± 30	167.8 ± 42	148.5 ± 37	151.7 ± 38	H176.2 ± 44	153 ± 38
^{48}V	16 d	11.5 ± 2.9	11.7 ± 2.9	L7.2 ± 1.8				H61.9 ± 16	
^{46}Sc	84 d	H10.7 ±2.8	10.1 ± 2.5	6.4 ± 1.6	4.8 ±1.2	L0.5 ± 0.1	7.7 ± 1.9	5.8 ± 1.4	8.6 ± 2.2
^{56}Co	77 d	L3.6 ± 0.9	H8.2 ± 2.0	6.6 ± 1.7					
^{24}Na	15 h	60.1 ±15.0							

Sample		**#11**	**#12**	**#14**	**#7**	**#10**	**#13**
Mass (kg)		0.0448	0.4581	0.3224	0.1052	0.2541	0.4421
Analysis Date		03 11 96	02 16 96	02 14 96	02 23 96	03 14 96	02 25 96
	$t_{1/2}$						
^{60}Co	5.3 a	H66.0 ± 6.6	5.1 ± 0.5	17.0 ± 1.7	16.2 ± 1.6	8.4 ± 0.8	17.3 ± 1.7
^{22}Na	2.6 a	H130.1 ± 13	72.8 ± 7.3	89.3 ± 8.9	95.4 ± 9.5	90.1 ± 9.0	83.3 ± 8.3
^{26}Al	700 ka	81.2 ± 4.1	57.0 ± 2.8	61.5 ± 3.1	54.9 ± 2.7	58.4 ± 2.9	63.6 ± 3.2
^{54}Mn	312 d						
^{48}V	16 d						
^{46}Sc	84 d						
^{56}Co	77 d						
^{24}Na	15 h						

preatmospheric meteoroid radius, the activities of measured St-Robert fragments were found to be systematically enriched in ^{26}Al relative to ^{60}Co and ^{22}Na, while ^{60}Co *vs.* ^{22}Na activities are grossly consistent and well correlated relative to the model predictions. Since ^{60}Co and ^{22}Na have short half-lives relative to ^{26}Al, the former are susceptible to recent variations in GCR levels. As a result of solar modulation effects, these short-lived isotopes should be depressed compared to model values, which are appropriate to the long-term, average GCR flux, and this effect probably explains the apparent enrichment in ^{26}Al.

To agree with the relative model results for ^{22}Na *vs.* ^{26}Al, activity in ^{22}Na must be systematically raised by 15–20% over observed levels. A correction is more difficult to derive for ^{60}Co due to its steep production profile as a function of depth. Comparing the highest activity levels observed in ^{22}Na and bearing in mind effects due to solar modulation, agreement with the observations is not possible for bodies >~65 cm using the model of Bhandari *et al.* (1993), where peak activity in ^{22}Na (for an average GCR flux) falls below 100 dpm/kg for bodies larger than this radius. A similar result is found for ^{26}Al, where maximum theoretical activities fall below 60 dpm/kg for radii in excess of 65 cm. This maximum radius corresponds to a spherical meteoroid of mass ~4000 kg.

The ^{60}Co results can be used to constrain the minimum size of the preatmospheric body. The Co activity indicates that the minimum value for the original preatmospheric mass of St-Robert was in the 500 to 1000 kg range, which is based on comparison with other falls and from model results (Eberhardt *et al.*, 1963; Spergel *et al.*, 1982). The low ^{56}Co activity indicates no exposure to solar cosmic rays and implies a sizable preatmospheric body (Evans *et al.*, 1987; Nishiizumi *et al.*, 1990), which is consistent with the ^{60}Co results. Sample #11 had the highest ^{60}Co activity (66 dpm/kg), which if it was near the center of a spherical preatmospheric body, implies a preatmospheric radius of at least ~36 cm or a mass of ~700 kg using the results of Eberhardt *et al.* (1963). For comparison, the ^{60}Co activities of Dhajala (H4, >45 kg) and Lost City (H5, >17 kg, preatmospheric mass 163 ± 5 kg; Ceplecha, 1996) are 6 to 14 dpm/kg and <1 dpm/kg, respectively, while larger meteorites, such as Jilin (H5, ≥4000 kg) and Allende (CV3, ≥2000 kg) have ^{60}Co activities in the ranges of 55–215 and 23–179 dpm/kg, respectively (Honda *et al.*, 1961; Evans *et al.*, 1982).

The high absolute activities in most spallogenic nuclei in St-Robert (particularly ^{26}Al) are difficult to explain particularly in light of the fall having occurred so close to solar maximum. Unusual chemistry, exposure history or a significantly nonspherical preatmospheric body may be partial explanations, but more information is clearly needed. Additional noble gas work and cosmic-ray track studies would prove invaluable in this regard.

CONCLUSIONS

Based on eyewitness accounts and IR satellite observations of the fireball that resulted in the St-Robert meteorite shower, the most probable azimuth for the ground path was found to be 202° ± 5° with a slope of 58° ± 3° from the horizontal. These values for the atmospheric trajectory result in a range of probable heliocentric orbits characterized by perihelion extremely close to the Earth's orbit and of low inclination, with a most likely entry velocity of ~13 km/s (12.7–13.3 km/s). The difference of 35° in derived entry slope between the satellite and visual observations underscores the imprecision of the latter.

From the optical satellite observations and an assumed bolometric efficiency of near 10%, a preatmospheric mass of slightly >1500 kg results. The independent methods of estimating the initial mass of the St-Robert meteoroid are summarized in Table 6. Based on acoustic measurements of the blast wave, the range of possible masses is 1000–100,000 kg with a most probable value of 10,000 kg. This estimate, however, is highly uncertain. From theoretical modeling of the fireball trajectory and incorporating the observed fragmentation behavior of the body, we believe the initial mass to be 1600 kg with possible values ranging from 1400–2000 kg within the limits of that model. Cosmogenic nuclide data produce a lower limit of 700 kg for the preatmospheric mass and an upper limit near 4000 kg. Using the derived velocity and initial mass estimates from the various techniques, it appears that satellite bolometric efficiencies for this event are close to the estimated value of 10% within a factor of 2 given the error limits of this analysis. The seismic coupling for this fireball is very small with $\approx 10^{-7}$ of the total energy transferred into the ground.

TABLE 6. Summary of results for mass and size of the St-Robert meteoroid based on various techniques.

Technique	Initial mass estimate (kg)	Range (kg)	Equivalent radii for spherical meteoroid (cm)
Optical Light Curve	1 500	500–3000	46 (32–58)
Acoustic Energy	~10^4	10^3–10^5	90 (40–190)
Theoretical Entry Model	1 600	1400–2000	47 (45–52)
Cosmogenic Nuclide	>700	700–4000	36–65
Mass on the Ground	>100		>19

We conclude that the St-Robert meteoroid was ~1500–2000 kg before entry with a radius of 45–50 cm. Based on the recovered mass in the field, it is estimated that ~100 kg of material landed in the form of centimeter-sized and larger fragments of which 25.4 kg has been recovered to date. The meteoroid moved in a prograde orbit of low inclination and encountered the Earth at its descending node. Additionally, many hundreds of kilograms of meteoric dust probably fell below and down wind of the detonation point.

Based on satellite data and modeling of the dark-flight portion of the path, the body fragmented extensively at least once near 36 km altitude under ram pressures of ~9 bars and produced a light flash of equivalent visual absolute magnitude, –18 at this height. The estimated end-height is near 25 km. The ground point of the detonation was 73.06° ± 0.01° west longitude and 45.84° ± 0.01° north latitude.

Thus satellite observations offer the potential to derive masses and orbits of Earth-crossing meteoroids which are beyond the detection limits of current telescopic search programs. Having ground truth from the St-Robert meteoroid allows calibration of satellite observations both phenomenologically and on a theoretical level. For example, McCord *et al.* (1995) calculated a mass range of 5×10^5–9×10^6 kg for the 1994 Feb 1 fireball event as observed by satellite sensors. This event was both faster and larger than St-Robert, and, thus, the bolometric efficiency factor of ~10% found from our observations (using a 6000 K blackbody model) is a lower limit for the 1994 Feb 1 event as this efficiency increases with mass and velocity (Nemtchinov *et al.*, 1995; Halliday *et al.*, 1981). From these considerations, we derive an upper limit of the mass for that meteoroid near 5×10^5 kg, which corresponds to a chondritic body <6 m in diameter.

Acknowledgements–We are very grateful to all the residents of eastern Canada and the United States who described the St-Robert fireball and to all the residents of the parishes of St-Robert and St-Aimé who loaned their meteorites for analysis and/or gave permission for searches of their farms.

Assistance provided by members of the Montreal Planetarium and members of the Fédération des Astronomes Amateurs du Québec in locating eyewitnesses was invaluable as was the assistance of P. Senecal of the International Meteor Organization. We also thank R. Herd, D. Thibault, G. Le Cheminant, A. Therriault and B. Robertson of the Geological Survey of Canada for locating eyewitnesses and providing other support for the investigation. D. Brueckner, C. Hale, J. Hanes, J. Irwin, H. Jamieson, S. Kissin, S. Legrand, D. Lemay, M. Nadeau, H. Plotkin, J. Rucklidge and P. Sicotte were cheery participants in the fieldwork. Enormous local support was provided by P. Sasseville. Upper wind data were supplied by the Climate Information Branch of Environment Canada and the National Climate Data Centre of the National Oceanic and Atmospheric Administration. Computer code for modeling was kindly provided by Z. Ceplecha. Helpful discussions with Z. Ceplecha and G. Herzog are gratefully acknowledged as are reviews by R. Hawkes and T. McCord. D. Niehaus made the corrected aerial photo mosaic for Fig. 7. We give special thanks to the United States Department of Defense for making satellite data available for this study. Funding for this research, as provided by the Canadian Space Agency through the Meteorites and Impacts Advisory Committee, is gratefully acknowledged. JW's work was supported by NASA Contract NASW-4841. This is GSC contribution number 35995 and LANL Contribution number LA-UR-96-0008.

Editorial handling: G. Wetherill

REFERENCES

ALLEN C. W. (1973) *Astrophysical Quantitites*. The Athlone Press, London. 310 pp.

ASTAPOVICH I. S. (1946) The Power of the Sound Detonations of the Choulak-Kurgan Bolide. *Byull. Turkin. FAN USSR* **2**, 77–80 (Technical Translation by Air Technical Intelligence Center, Wright-Patterson Air Force Base, Ohio, ATIC-242107,F-TS-8844/III).

AYERS W. G., MCCROSKY R. E. AND SHAO C. Y. (1970) Photographic Observations of ten artificial meteors. Smithsonian Astrophys. Observ. Special Rep. 317 pp.

BHANDARI N., MATHEW K. J., RAO M. N., HERPERS U., BREMER S., VOGT S., WOLFLI W., HOFMANN H. J., MICHEL R., BODEMAN R. AND LANGE R.-J. (1993) Depth and Size dependence of cosmogenic nuclide production rates in stony meteoroids. *Geochim. Cosmochim. Acta.* **57**, 2361–2375.

BOROVICKA J. (1990) The comparison of two methods of determining meteor trajectories from photographs. *Bull. Astron. Inst. of Czech.* **41**, 391–396.

BOROVICKA J. (1993) A fireball spectrum analysis. *Astron. Astrophys.* **279**, 627–645.

BOROVICKA J. (1994) Two components in meteor spectra. *Planet. Space. Sci.* **42**, 145–150.

BRODZINSKI R. L. (1973) The use of gold as a backscatter absorber in multidimensional gamma ray spectrometers. *Radiochem. Radioanal. Lett.* **13**, 375–380.

BROWN P., CEPLECHA Z., HAWKES R., WETHERILL G. W., BEECH M. AND MOSSMAN K. (1994) The Orbit and atmospheric trajectory of the Peekskill meteorite from video records. *Nature* **367**, 624–626.

CEPLECHA Z. (1961) Multiple Fall of Pribram Meteorites Photographed. *Bull. Astron. Inst. of Czech.* **12**, 21–47.

CEPLECHA Z. (1987) Geometric, Dynamic, Orbital and Photographic Data on Meteoroids from Photographic Fireball Networks. *Bull. Astron. Inst. of Czech.* **38**, 222–234.

CEPLECHA Z. (1996) Luminous Efficiency based on photographic observations of the Lost City fireball and implications to the influx of interplanetary bodies onto Earth. *Astron. Astrophys.*, in press.

CEPLECHA Z., SPURNÝ P., BOROVICKA J. AND KECLÍKOVÁ J. (1993) Atmospheric Fragmentation of Meteoroids. *Astron. Astrophys.* **279**, 615–626.

COX E. F. (1958) Sound Propagation in Air. *HandBuch der Physik* **XLVIII**, 455–478.

CUMMING G. L. (1989) Alberta Bolide of April 1, 1982: Interpretation of photographic and seismic records. *Can. J. Earth. Sci.* **26**, 1350–1355.

DAVIDSON M. AND WHITAKER R. W. (1992) Miser's Gold. LA-12074-MS, UC-741, (available from NTIS, U.S. Dept. of Commerce, Springfield, Virginia) 28 pp.

DUMOND J. W. M., COHEN E. R., PANOFSKY W. K. H. AND DEEDS E. (1946) A Determination of the Wave Forms and Laws of Propagation and Dissipation of Ballistic Shock Waves. *J. Acous. Soc. Amer.* **18**, 97–118.

EBERHARDT P., GEISS J. AND LUTZ H. (1963) Neutrons in meteorites. In *Earth Science and Meteoritics* (eds. J. Geiss and E. D. GoldBerg), 143–168. North-Holland Publishing Co., Amsterdam.

EDWARDS D. R., REEVES J. H. AND BRODZINSKI R. L. (1982) Preparation of lunar sample and meteorite mock-ups: Or how to make rocks. *Nucl. Instrum. Methods* **196**, 507–509.

EVANS J. C. AND REEVES J. H. (1987) ^{26}Al survey of Antarctic meteorites. *Earth Planet. Sci. Lett.* **82**, 223–230.

EVANS J. C., REEVES J. H., RANCITELLI L. A AND BOGARD D. D (1982) Cosmogenic radionuclide variations in recently fallen meteorites: Evidence for galactic cosmic ray variations during the period 1967–1978. *J. Geophys. Res.* **87 (B7),** 5577–5591.

EVANS J. C., REEVES J. H. AND REEDY R. C. (1987) Solar cosmic ray produced radionuclides in the Salem meteorite (abstract). *Lunar Planet. Sci.* **18,** 271–272.

FEW A. A. (1969) Power Spectrum of Thunder. *J. Geophys. Res.* **74**, 6926–6934.

FOLINSBEE R. E. AND BAYROCK L. A. (1961) The Bruderheim meteorite–Fall and recovery. *J. Roy. Astron. Soc. Can.* **55**, 218–228.

FUJIWARA A., CERRONI D. R., DAVIS E., RYAN M., DI MARTINO M., HOLSAPPLE K. AND HOUSEN K. (1989) Experiments and Scaling Laws on Catastrophic Collisions. In *Asteroids II* (eds. R. P. Binzel, T. Gehrels and M. S. Matthews), pp. 240–269. Univ. Arizona Press, Tucson, Arizona.

GOLD T. AND SOTER S. (1979) Bronstides: Natural Explosive Sounds. *Science* **204**, 371–375.

GRIFFIN A. A., MILLMAN P. M. AND HALLIDAY I. (1992) The Fall of the Abee Meteorite and its probable orbit. *J. Roy. Astron. Soc. Can.* **86**, 5–14.

HALLIDAY I. (1983) Meteorite orbits from observations by camera networks. In *Highlights of Astronomy* (ed. R. M. West), pp. 399–405. 28th General Assembly of the International Astronomical Union, Reidel, Dordrecht, The Netherlands.

HALLIDAY I. (1985) The Grande Prairie Fireball of 1984 February 22. *J. Roy. Astron. Soc. Can.* **79**, 197–215.

HALLIDAY I. AND MCINTOSH B. A. (1990) Orbit of the Murchison Meteorite. *Meteoritics* **25**, 339–340.

HALLIDAY I., BLACKWELL A. T. AND GRIFFIN A. A. (1978) The Innisfree Meteorite and the Canadian Camera Network. *J. Roy. Astron. Soc. Can.* **72**, 15–39.

HALLIDAY I., GRIFFIN A. A. AND BLACKWELL A. T. (1981) The Innisfree Meteorite Fall: A Photographic Analysis of Fragmentation, Dynamics and Luminosity. *Meteoritics* **16**, 153–170.

HALLIDAY I., BLACKWELL A. T. AND GRIFFIN A. A. (1989a) The typical meteorite event, based on photographic records of 44 fireballs. *Meteoritics* **24**, 65–72.

HENDERSON H. R. AND HILTON D. A. (1974a) Sonic-Boom Ground Pressure Meaasurements from the Launch and Reentry of Apollo 16. NASA TN D-7606. 43 pp.

HENDERSON H. R. AND HILTON D. A. (1974b) Sonic-Boom Measurements on the FocusRegion During the Ascent of Apollo 17. NASA TN D-7806. 33 pp.

HILTON D. A., HENDERSON D. A. AND MCKINNEY R. (1972) Sonic-Boom Ground-Pressure measurements from Apollo 15. NASA TN D-6950. 35 pp.

HONDA M. S., UMEMOTO S. AND ARNOLD J. R. (1961) Radioactive species produced by cosmic rays in Bruderheim and other stone meteorites. *J. Geophys. Res.* **66**, 3541–3546.

JENNISKENS P., BOROVICKA J., BETLEM H., TER KUILE C., BETTONVIL F. AND HEINLEIN D. (1992) Orbits of meteorite producing fireballs. *Astron. Astrophys.* **255**, 373–376.

JENNISKENS P., BETLAM H., BETLAM J., BARIFAIJO E., SCHLUTER T., HAMPTON C., LAUBENSTEIN M., KUNZ J. AND HEUSSER G. (1994) The Mbale meteorite shower. *Meteoritics* **29**, 246–254.

KEAY C. S. L. (1992) Electrophonic sounds from large meteor fireballs. *Meteoritics* **27**, 144–148.

KRINOV E. L. (1960) *Principles of Meteoritics.* Pergamon Press, New York. 535 pp.

LEVIN B. J. AND SIMONENKO A. N. (1969) Meteorite Radiants and Orbits. In *Meteorite Research* (ed. P. M. Millman), pp. 552–559. D. Reidel, Dordrecht, The Netherlands.

MCCORD T. B., MORRIS J., PERSING D., TAGLIAFERRI E., JACOBS C., SPALDING R., GRADY L. AND SCHMIDT R. (1995) Detection of a meteoroid entry into the Earth's atmosphere on February 1, 1994. *J. Geophys. Res.* **100**, 3245–3249.

MCCROSKY R. E., POSEN A., SCHWARTZ G. AND SHAO C.-Y. (1971) Lost City Meteorite–Its recovery and a comparison with other fireballs. *J. Geophys. Res.* **76**, 4090–4108.

MCCROSKY R. E., SHAO C.-Y. AND POSEN A. (1976) Prairie Network fireball data I. Summary and orbits. Centre for Astrophysics Preprint Series, No. 655, Cambridge, Massachusetts. 13 pp.

McIntosh B. A. and Douglas J. A. V. (1967) The Fireball of April 25, 1966. I, Canadian Visual Observations. *J. Roy. Astron. Soc. Can.* **61**, 159–178.

Michel R., Dragovitsch P., Cloth P., Dagge G. and Filges D. (1991) On the production of cosmogenic nuclides in meteoroids by galactic protons. *Meteoritics* **26**, 221–242.

Miley H. S., Brodzinski R. L. and Reeves J. H. (1992) Low-background counting systems. *J. Radioanal. Nuc. Chem.* **160**, 371–385.

Nemtchinov I. V., Spalding R. E., Jacobs C., Tagliaferri E., Artem'eva N. A., Golub A. P., Kosarev I. B., Popova O. P., Svettsov V. V. and Shuvalov V. V. (1995) Assessment of the Large Meteoroid Characteristics from the Light Curves Obtained by Satellite and GroundBased Networks (abstract). *Meteoritics* **30**, 556.

Nininger H. H. (1952) *Out of the Sky.* Dover Publications, Mineola, New York. 336 pp.

Nishiizumi K., Nagai H., Imamura M., Honda M., Kobayashi K., Kubik P. W., Sharma P., Wieler R., Signer P., Goswami J. N., Sinha N., Reedy R. C. and Arnold J. R. (1990) Solar cosmic ray produced nuclides in the Salem meteorite (abstract). *Meteoritics* **25**, 392.

Passey Q. R. and Melosh H. J. (1980) Effects of Atmospheric Breakup on Crater Field Formation. *Icarus* **42**, 211–233.

Perkins R. W., Rancitelli L. A., Cooper J. A., Kaye J. H. and Wogman N. A.(1970) Cosmogenic and primordial radionuclide measurements in Apollo 11 lunar samples by nondestructive analysis. *Proc. Apollo 11 Lunar Sci. Conf.*, 1455–1469.

Qamar A. (1995) Space shuttle and meteroid [sic]—tracking supersonic objects in the atmosphere with seismographs. *Seismol. Res. Lett.* **66**, 6–12.

Reed J. W. (1966) Amplitude Variability of Explosion Waves at Long Ranges. *J. Acous. Soc. Amer.* **39**, 980.

Reed J. W. (1972) Attenuation of Blast Waves in the Atmosphere. *J. Geophys. Res.* **77**, 1616.

Reed J. W. (1977) Atmospheric Attenuation of Explosion Waves. *J. Acous. Soc. Amer.* **61**, 39.

Reeves J. H., Hensley W. K., Brodzinski R. L. and Ryge P. (1984) An ultralow background germanium gamma-ray spectrometer using superclean materials and cosmic ray anticoincidence. *IEEE Trans. Nuclear Sci.* **NS-31**, 697.

Revelle D. O. (1976) On Meteor-Generated Infrasound. *J. Geophys. Res.* **81**, 1217.

Revelle D. O. (1980) A Predictive Macroscopic Integral Radiation Efficiency Model. *J. Geophys. Res.* **85**, 1803.

Revelle D. O. and Whitaker R. W. (1996) Acoustic efficiency analysis using infrasound from NEOs, LAUR-95-4121. *Proc. Space Conf.*, in press.

Spergel M. S., Reedy R. C., Lazareth O. W. and Levy P. W. (1982) Cosmic ray-produced cobalt 60 in chondrites (abstract). *Lunar Planet. Sci.* **13,** 756–757.

Spergel M. S., Reedy R. C., Lazareth O. W., Levy P. W. and Slatest L. A. (1986) Cosmogenic neutron-capture-produced nuclides in stony meteorites. *Proc. Lunar Planet. Sci. Conf.* **16th,** 483–494.

Tagliaferri E., Spalding R., Jacobs C., Worden S. P. and Erlich A. (1994) Detection of meteoroid impacts by optical sensors in Earth orbit. In *Hazards Due to Comets and Asteroids.* (ed. T. Gehrels) pp. 199–220. Univ. Arizona Press, Tuscon, Arizona.

Wetherill G. W. (1968) Stone Meteorites: Time of Fall and Origin. *Science* **169**, 79–82.

Wetherill G. W. and Revelle D. O. (1981) Which fireballs are meteorites? *Icarus* **48**, 308–328.

Wetherill G. W. and Chapman C. R. (1988) Asteroids and Meteorites. In *Meteorites and the Early Solar System* (eds. J. Kerridge and M. S. Matthews), pp. 35–71. Univ. Arizona Press, Tucson, Arizona.

White R. (1984) *Canadian Meteorites.* Provincial Museum of Alberta, Edmonton. 43 pp.

Wilson G. C. (1994) Mineralogy, Chondrule types, Textures and Optical Classification of the St-Robert Meteorite Fall. Technical Report, Isotrace Laboratory, Toronto, Canada. 15 pp.

Wogman N. A., Robertson D. E. and Perkins R. W. (1967) A larger detector, anticoincidence shielded multidimensional gamma-ray spectrometer. *Nucl. Instrum. Methods* **50**, 1–10.

Wogman N. A., Perkins R. W. and Kaye J. H. (1970) An all sodium iodide anticoincidence shielded multidimensional gamma-ray spectrometer for low activity samples. *Nucl. Instrum. Methods* **83**, 277–282.

Zepler E. E. and Harel J. R. P. (1965) The Loudness of Sonic Booms and Other Impulsive Sounds. *J. Sound and Vibr.* **2**, 249.